AN ABSTRACT OF THE THESIS OF

Paris Kalathas for the degree of Master of Science in Computer Science presented on June 14, 2019.

Title: Dynamic Analysis and Comparison of High-Rise Building Frames Made of Mass-Timber and Traditional Materials Using Finite Element Analysis

Abstract approved: _____

Yue Zhang

The increased demand for building materials that are friendly to the environment, along with the latest advances in wood science and technology, which exploit the fiber orientation of wood, resulted in composite wood materials known as mass-timber products. To understand the effects the wood fiber orientation has on the dynamic behavior of buildings and on vibration comfort, we examine twenty four high-rise building frames made from four different structural materials: conventional wood (Douglas-Fir), glued laminated timber (GluLam), cross laminated timber (CLT), steel and concrete. Utilizing the well-established Finite Elements Analysis (FEA), we study the building frames using a modal, a modal dynamics, an impulse response and an earthquake response analyses. These experiments revealed information about the frames such as natural frequencies (modes), resonance displacement, damping ratio, load propagation and dynamic response due to earthquake excitation. The results show that mass timber products, GluLam and CLT, when combined together demonstrate exceptional dynamic behavior, resulting in higher damping coefficients and reduced floor displacements compared to the other materials. However, they exhibited vibrations at a high frequency range, a behavior that needs further investigation in order to evaluate how it affects the integrity and longevity of the building frames.

Dynamic Analysis and Comparison of High-Rise Building Frames Made of Mass-Timber and Traditional Materials Using Finite Element Analysis

by
Paris Kalathas

A THESIS

submitted to

Oregon State University

in partial fulfillment of
the requirements for the
degree of

Master of Science

Presented June 14, 2019
Commencement June 2020

Master of Science thesis of Paris Kalathas presented on June 14, 2019

APPROVED:

Major Professor, representing Computer Science

Head of the School of Electrical Engineering and Computer Science

Dean of the Graduate School

I understand that my thesis will become part of the permanent collection of Oregon State University libraries. My signature below authorizes release of my thesis to any reader upon request.

Paris Kalathas, Author

ACKNOWLEDGEMENTS

Foremost, I would like to thank and express my appreciation to my advisor Dr. Yue Zhang for all the guidance and support throughout these years. Next, I would like to thank Dr. Ben Lee for the guidance he gave me as a professor and as committee member, Dr. Mike Bailey for his guidance as a professor and committee member as well as for allowing me to work with his equipment for this research, and Dr. Lizhong Chen for serving my committee and selecting me as one of his teaching assistants. Likewise, I would like to thank Dr. Arijit Sinha and Dr. Ben Mason for the knowledge and suggestions they provided for this research, and Ms. Leanne Lai and Mr. Mike Sanders for all their help for the software and hardware equipment. Finally, I would like to thank my family and friends for all their support during this journey.

TABLE OF CONTENTS

TABLE OF CONTENTS (Continued)

Page

LIST OF FIGURES

LIST OF FIGURES (Continued)

Figure Page

LIST OF TABLES

LIST OF EQUATIONS

Chapter 1: Introduction

Recent technology advances have introduced new methods of timber processing allowing the fabrication of mass-timber columns, beams and panels, including Glue Laminated timber (GluLam), Cross Laminated Timber (CLT) and Nail Laminated Timber (NLT), Fig. 1.1. GluLam is a fabricated composite wood with its fibers been parallel to each other between its layers, which are glued together. In the construction industry, GluLam is mainly used for the construction of beams and columns. CLT is a wood composite with its fibers oriented perpendicular to each other between its layers, which are glued together. Its use in the industry is mainly for floor slabs and shear walls. NLT is similar to GluLam with the only difference that its layers are nailed or screwed together. Composite wood products differ from traditional wood products by having increased stiffness, which pushes forward the wooden structures' boundaries, making possible the construction of buildings of five stories and above.

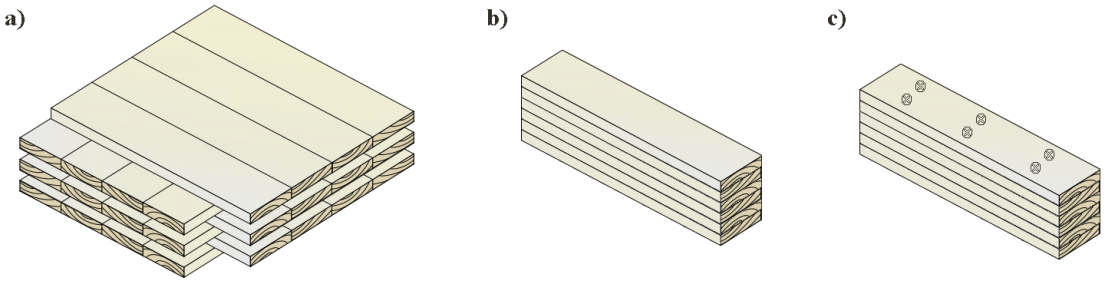

Figure 1.1: Mass timber products, United States Department of Agriculture (2013).

Wooden structures have been proven superior when compared to masonry structures, resulting to 15% to 40% energy savings due to thermal resistance they offer. In addition, wood as an environmental-friendly sustainable material demonstrates the lower embodied energy when compared to traditional construction materials such as steel, concrete and bricks, Asdrubali et al. (2016). However, the material complexity and the architecture design that comes along with those buildings require rigorous analyses to ensure the building's rigidity and tolerance to the environmental elements such as winds, earthquakes and fires. Furthermore, research is needed to ensure compliance with the current standards for acoustic and vibration comfort in living environments, which demand the limitation of the building's vibrations below certain amplitude and frequency, Schiavia and Rossi (2015), Kawecki et al. (2011), Kawecki and Kowalska (2011). Currently, part of the ongoing research from the engineering community focuses on investigating new methods to predict and control vibrations on structures to avoid structural failure and residents' disturbance. From a different perspective, researchers investigate ways to harvest building vibrations using piezo-electric materials, which can potentially contribute as green energy resource, Wei and Jing (2017), Amini et al. (2017).

Chapter 2: Background

2.1 Mechanical Material Properties

The properties of every material are essential in physical and in numerical terms for modeling calculations. In this section the mechanical material properties are explained briefly as they are being used in this thesis for the numerical models in the FEA calculations. Density, denoted as ρ, refers to the material volumetric mass m contained in a certain volume V. It is expressed in kg/m^3 and it is calculated as,

$$\rho = \frac{m}{V} \tag{2.1.1}$$

Young's modulus or elasticity E refers to a material's elastic deformation on an axis under load. High E values translate to stiff materials, where low values reveal soft materials. Young's modulus is expressed in pascals Pa and it is calculated using Equation 2.1.2, where σ is the stress and ε the strain in the direction of the applied load.

$$E_x = \frac{\sigma_x}{\varepsilon_x} \tag{2.1.2}$$

The Poisson effect refers to the reaction of a material at the different sides of the compression axis and the dimensionless Poisson's number v shows the ratio of longitudinal to lateral deformations with respect to a certain axis, numerically expressed as,

$$v_{xy} = -\frac{\partial \varepsilon_z}{\partial \varepsilon_x} \tag{2.1.3}$$

Shear modulus *G* is the ratio of shear stress to the shear strain. It is expressed in pascals *Pa* and calculated as,

$$G_{xy} = \frac{\tau_{xy}}{\gamma_{xy}} \tag{2.1.4}$$

where, τ is the stress and γ the strain in the direction of the applied load.

Finally, damping ζ expresses the energy loss in an oscillating system, causing its displacement to be reduced to zero. Examples of damping in classical mechanics are hysteresis damping, viscous damping and modal damping. In this study we calculated the frames' hysteresis damping using the logarithmic decrement method. Figure 2.1.1 shows the oscillation of a body over time after an impulsive excitation. The maximum displacement *X* at each period of the oscillation can be used to calculate the logarithmic decrement δ, Eq. 2.1.5. Then, using the logarithmic decrement we can calculate the damping ζ, Eq. 2.1.6.

$$\delta = \frac{1}{n} ln \frac{x(t)}{x(t+nT)} \tag{2.1.5}$$

$$\zeta = \frac{1}{\sqrt{1 + \left(\frac{2\pi}{\delta}\right)^2}} \tag{2.1.6}$$

Where, *n* is the number of periods between peaks and *T* the period of the oscillation.

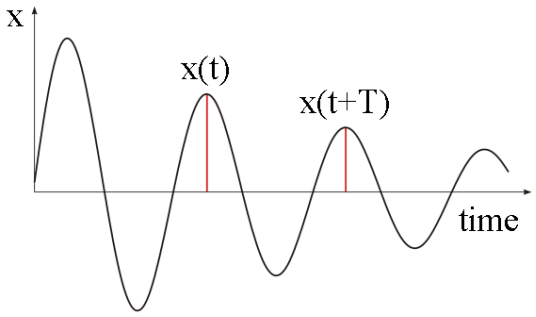

Figure 2.1.1: The oscillation displacement of a body over time.

2.2 Material Categories

Based on their properties, including mechanical, electrical or optical, materials can be categorized for specific usage. Figure 2.2.1 shows the two main material categories, isotropic (a) and anisotropic (b) as well as the orthotropic (c) category, which is a subset of the anisotropic materials. Taking as an example the Young's modulus *E*, each point in an isotropic material as the same *E* for every axis, $E_{xi}=E_{yi}=E_{zi}$ i=1,2,3…# of points. Examples of materials that belong in this category are metals and glass. On the contrary, anisotropic materials are those whose each point has different *E* from every other point and for every axis, $E_{xi}\neq E_{yi}\neq E_{zi}\neq E_{xi}\neq E_{xk}\neq E_{xm}\neq E_{yi}\neq E_{yk}\neq E_{ym}\neq E_{zi}\neq E_{zk}\neq E_{zm}$ i,k,m=1,2,3…# of points. Some examples of anisotropic materials are crystals and fiber reinforced solids. Orthotropic materials have different *E* on each axis, but for each point the *E* remains the same for each axis, $E_{xi}\neq E_{yi}\neq E_{zi}$, $E_{xi}=E_{xk}=E_{xm}$, $E_{yi}=E_{yk}=E_{ym}$, $E_{zi}=E_{zk}=E_{zm}$ i,k,m=1,2,3…# of points. Wood is an example of orthotropic material.

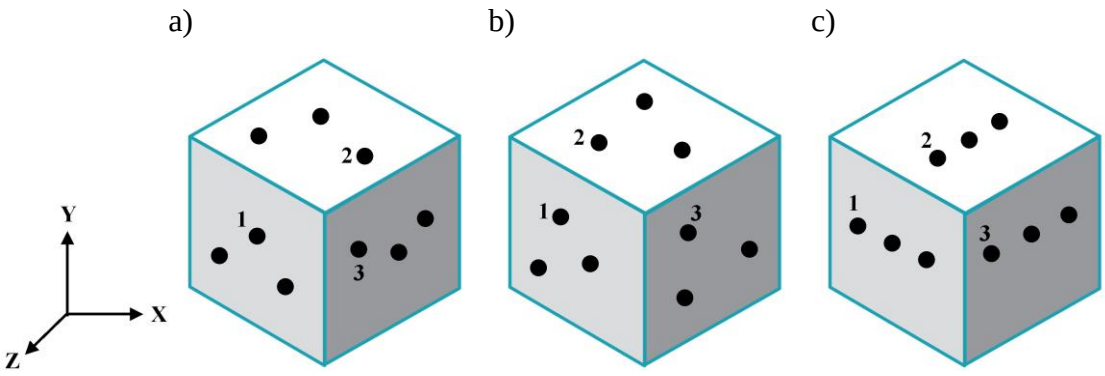

Figure 2.2.1: Isotropic (left), anisotropic (middle) and orthotropic (right) materials.

2.3 Finite Element Analysis/Method: Overview

The Finite Element Analysis/Method (FEA/FEM) was developed around the idea of discretizing the physical bodies under investigation and examine their behavior in the temporal and spatial domain. Figure 2.3.1 shows the overall procedure of solving physical problems using FEA. The procedure begins with stating the physical problem, and its mathematical representation can be formed after making the right assumptions, providing the description of the problem at its equilibrium position. This includes representations for the geometries, material laws, loads, boundary conditions and other parameters depending on the problem. The next step is to discretize the geometries to finite elements (FE), which are constructed using nodes and connecting them with edges. The numerical representation of a physical body using nodes and edges is called "Mesh". The resolution of the mesh depends on the analysis and it can affect the accuracy and the memory space needed for the results. For the selection of the appropriate mesh size, sensitivity studies should be performed to examine the output changes when different meshes are chosen. In addition, the mesh can be further optimized on regions where phenomena of special interest may occur. Figure 2.3.2

shows examples of a 2D mesh and how it can be refined for the whole body and at specific areas to avoid calculation errors.

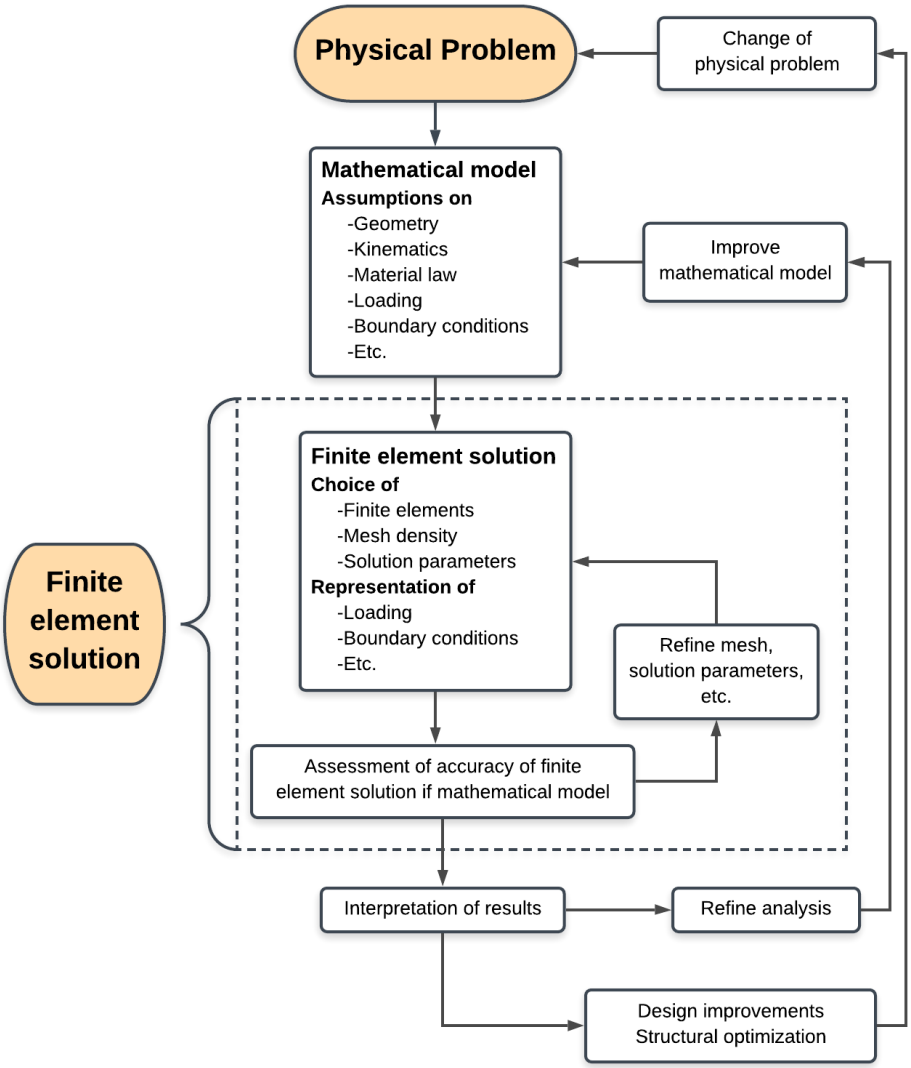

Figure 2.3.1: The FEA problem solving procedure, Bathe (2014).

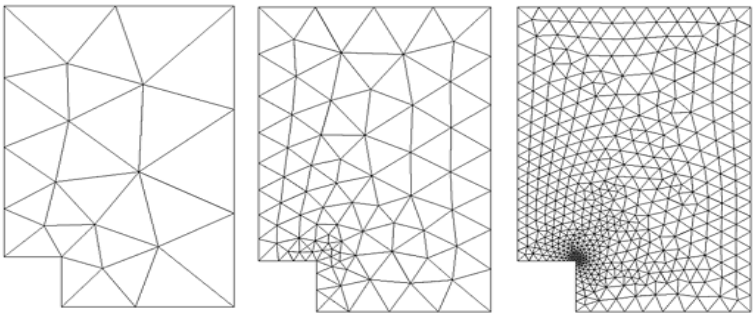

Figure 2.3.2: Coarse(left) to fine(right) FEA mesh, Frei (2013),.

Another parameter associated with the mesh are the mesh elements, Fig. 2.3.3. The mesh elements are closely related with the body under investigation, and they have different features associate with them. Examples of those features are the degrees of freedom (DOF) for each element, which allow or prevent movement at specific directions as well as the output variables that can be extracted from each element like stress, forces, acoustic pressure etc. It is possible on a single body to have different mesh elements according to the specific region of the geometry or different materials in the same geometry. After the geometry discretization, groups of nodes and/or surfaces can be created to assign the loads, boundary conditions, interactions and other properties needed to accurately define the problem.

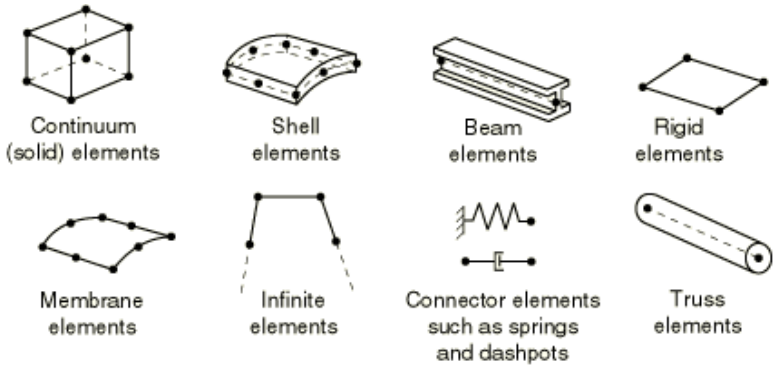

Figure 2.3.3: Various mesh elements, Simulia (2014).

Once the models are created and all the material parameters, contacts and loads are set, the right type of analysis must be selected. There are various types of analysis exist including static, dynamic, linear, non-linear, modal, heat transfer analysis etc. The main parameters associated with the analyses are the total time for the analysis and the time increment size for the calculations. Just like meshing, these are crucial parameters which affect the results, the calculation time and the memory space needed; therefore, sensitivity studies should be contacted to estimate their appropriate values.

2.4 Finite Element Analysis/Method: Mathematical Derivation

FEA is based on the weak formulation of a problem, which is the integral form of the governing equation for the system under investigation. Consider the 1D static state cantilever problem under stretch shown in Figure 2.4.1,

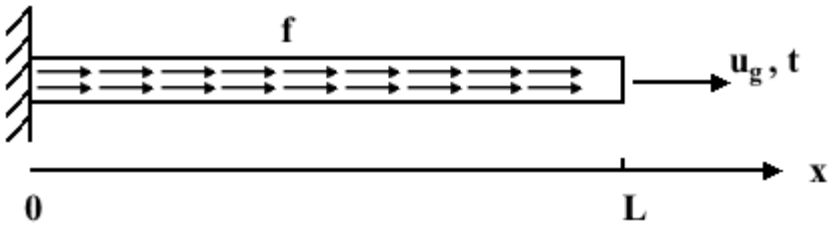

Figure 2.4.1: 1D cantilever.

where,

u_g : specified displacement at $x = L$
t: specified traction (force) at $x = L$
f: distributed body force

For this setting, the problem is to find $u(x) \in S = \{u \mid u(0) = u_0\}$ where $u(x)$ is a displacement function, and S is a function space,

given $u(0) = u_o,\ u_g\ or\ t, f(x)$ and constitutive relation $\sigma = E\frac{du}{dx}$, where, E is the Young modulus, such that

$$\frac{d\sigma}{dx} + f = 0 \quad \text{in (0, L)} \tag{2.4.1}$$

with boundary conditions $u(0) = u_o\ and\ u(L) = u_g\ or\ \sigma(L) = t$. We call the partial differential equation 2.4.1 the strong form of the partial differential equation. To be able to solve the equation using FEA, it needs to be converted to the weak (Galerkin) form. To do this, we want to find $u(x) \in S = \{u \mid u(0) = u_0\}$ where $u(x)$ is a displacement function, and S is a function space, given $u(0) = u_o,\ u_g\ or\ t, f(x)$ and constitutive relation $\sigma = E\frac{du}{dx}$ such that, $\forall\ w \in V = \{w \mid w(0) = 0\}$

$$\int_0^L \frac{dw}{dx}\sigma dx = \int_0^L wf dx + w(L)t \tag{2.4.2}$$

where, w is an arbitrary function, and V is a function space.

Using FEA we construct and solve approximations of the Equation 2.4.2 in finite-dimensional function spaces which are subsets of the infinite-dimensional spaces S and V, to find $u^h(x) \in S^h \subset S$ with $S^h = \{u^h \in H^1(0, L) \mid u^h(0) = u_o\}$ such that, $\forall w^h \in V^h \subset V$ with $V^h = \{w^h \in H^1(0, L) \mid w^h(0) = 0\}$ where, H^1 is a function space with basis functions that can be squared and integrated. In higher-dimension problems H^1 can be H^2, H^3 etc. Equation 2.4.3 is the finite-dimensional weak form. To obtain u^h and w^h we first partition the domain $(0, L)$ into subdomains, which are defined using the finite elements Ω^1, Ω^2, Ω^e and nodes x^1, x^2, x^N as shown in Figure 2.4.2.

$$\int_0^L \frac{dw^h}{dx}\sigma^h dx = \int_0^L w^h f dx + w^h(L)t \tag{2.4.3}$$

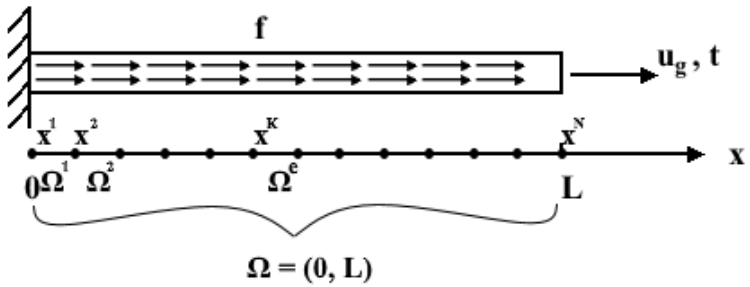

Figure 2.4.2: FEA partitioning. Finite subdomains (Ω) and nodes (x).

After partitioning, the weak form becomes

$$\int_{\Omega} \frac{dw^h}{dx}\sigma^h dx = \int_{\Omega} w^h f dx + w^h(L)t$$

$$\Rightarrow \sum_{e=1}^{N_{el}} \int_{\Omega^e} \frac{dw^h}{dx}\sigma^h dx = \sum_{e=1}^{N_{el}} \int_{\Omega^e} w^h f dx + w^h(L)t \qquad (2.4.4)$$

Once the finite elements are constructed, a finite number of local basis functions for $u(x)$ and w(x) can be defined for each element $\Omega^1, \Omega^2, \ldots \Omega^N$, and therefore over the whole domain Ω. Since the elements in the 1D cantilever problem are consist of two nodes, the basis functions are linear as shown in Figure 2.4.3 for a single element and in Figure 2.4.4 over the whole domain Ω, Garikipati (2014).

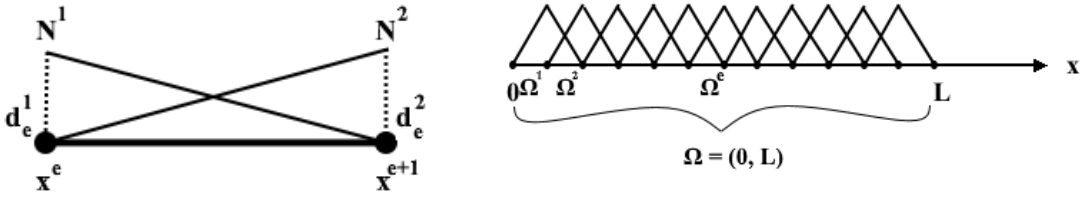

Figure 2.4.3: Basis functions on a single finite element (left) and over the entire problem domain (right).

Chapter 3: Literature Review

Natural modes, vibration response and damping coefficients are essential dynamic properties in construction engineering. To avoid structural failure and resident disturbance, engineers constantly investigate new methods to calculate, isolate and mitigate vibrations on buildings. Furthermore, national agencies form construction codes specifying the buildings' vibrations acceptable ranges for frequency and amplitude. Several studies have been made on dynamic analysis of CLT buildings using field measurements, lab experiments and computer modeling. Reynolds et al. (2015), examined the ambient vibrations and damping coefficient of a 7-story CLT building during construction. Acceleration measurements were taken in two different days during the construction process, at three points at an optimal region of the building. The results showed that the theoretical estimation for the fundamental frequency agrees with the measured frequency for day one; however, the measured frequency for day two is higher than the theoretical value. Furthermore, the measurements for the damping ratio showed values ranging from 3.2% to 5.6% for the first day, and 5.2% to 9.1% for day two, which indicates a level of uncertainty on the measurements. Mugabo et al. (2019) took vibration measurements from a four-story wooden building with dimensions 27.20 × 13.95 m floor area and 15.39 m height made of CLT floors and GluLam frame. The measurements were taken at the third and fourth floor and the frequency range for the vibrations was between 2.5 – 5.0 Hz, similar to the frequency range found in Hu et al. (2014) and Reynolds et al. (2014). Quang Mai et al. (2018) took measurements from CLT and hybrid slabs to examine how the added concrete layer and the connector placement and orientation affect the dynamic behavior of the slabs. The study concluded that the concrete layer increases the natural frequency of the slab from ~8 Hz to ~12 Hz.

Furthermore, the connector spacing and angle result to frequency differences 4.6% and 3.2% respectively.

Sandhaas and Ceccotti (2012), Popovski and Garvic (2015), Hristovski et al. (2013) and Sato et al. (2019), investigated the dynamic response and earthquake resistance of CLT structures involving the shaking-table technique. The structure used by Hristovski et al. (2013) had walls directly connected to the shaking table without a floor. The results from the application of various earthquake and sinusoidal forces showed strong vibrational activity at the zone of 1 - 3 Hz, and structural damping at 2.78%. Popovski and Garvic (2015) used a 2-story building for one push-over and four cyclic tests, Fig. 3.1. Measurements for the natural frequencies were taken before and after the tests showing a variation between 12.63 - 13.50 Hz and between 8.63 - 11.00 Hz respectively. These studies provided valuable information about the natural frequencies observed on CLT structures; however, they are limited to 1 and 2-story structures.

Figure 3.1: The 2-story building used for the tests in Popovski and Garvic (2015).

The FEA method has been utilized by several researchers for dynamic analysis on buildings. Edskär I. and Lidelöw H. (2019) calculated the natural frequencies of CLT, post and beam, and hybrid building frames with height ranking from 18 - 66 m using field measurements, computer simulation and theoretical calculations. The study showed frequencies in the range of 0.9 – 4.15 Hz, having FEA in close agreement with the field measurements. Furthermore, the authors found that to decrease acceleration magnitude on buildings with natural frequency below 1Hz added mass is needed, and for buildings with natural frequency above 2Hz it is recommended to increase the stiffness of the building.

To create accurate and representative models, Hyun and Young (2014) and Ventura et al. (2005) worked with both field measurements and FEA analysis. Hyun and Young (2014) studied the natural frequencies of 6 buildings with height ranging from 57 – 142 m, the equivalent of 18 – 45 story buildings, and Ventura et al. (2005) studied a 15-story building. Both studies performed calculations before and after optimization of the FE models with data collected from field measurements, such as values for Modulus of Elasticity, density, stiffness and moment of inertia. The initial FE models from Hyun and Young (2014) showed accuracy ranging from 53% - 98% and Ventura et al. (2005) found the first vibration mode accuracy to be 84.3%. After calibration, the models showed accuracy 83% - 100% and 99% for the two studies respectively. The results from these studies show that the dynamic behavior of mass-timber structures can be accurately predicted utilizing FEA analysis; however, design modifications that occur during the construction such as additional structural elements or changes on the materials, should be included on the FE models as well, and the analyses should be repeated.

Jarnero et al. (2010) examined the differences on CLT slabs' vibration properties when these are measured in the lab, at the construction zone and when they are calculated using computer simulation. The results showed variations between the measurements due to additional constraints that occurred from the walls after the slabs are installed on the building, and due to modeling simplifications of the computer simulation. The outcome from this study complements the results from the studies analyzed previously, which indicate that major changes may occur on the dynamic response of the slabs between laboratory measurements, FEA modeling and after/during the construction.

Gsell et al. (2007), Ussher et al. (2017), Weckendorf et al. (2016), Ussher et al. (2017) and Maldonado and Chui (2014) investigated the effects of the slab design on the dynamic response of CLT floors. Lab experiments were used along with FEA, achieving close agreement between the two methods. These studies used a simplified thin shell element modeling, which can reduce the calculation time and the memory space required for the simulation. While this method of modeling can examine accurately natural frequencies and vibrations for simple slab models, complex models, including buildings frames require 3D elements with sufficient number of nodes. This approach is needed to accurate capture the structure's dynamic behavior, avoiding artificial stiffness and mismatches on the degrees of freedom between the nodes when constraints and interactions are applied, Izzi et al. (2018). Our method solves this problem by constructing the mass-timber parts using individual wooden slabs made of C3D8R elements, which are 3D brick elements with 8 nodes available for the calculations.

Currently, the literature on modal and dynamic behavior of CLT buildings is limited in number, variety, and with small number of specimens. In this study we investigate the effect of materials on the modal parameters including the natural frequencies and damping coefficients of twenty-four building frames. Furthermore, the study examines the behavior of the frames when they are excited at their fundamental frequency, and how these frames respond to random excitations like earthquakes.

Chapter 4: Numerical Method

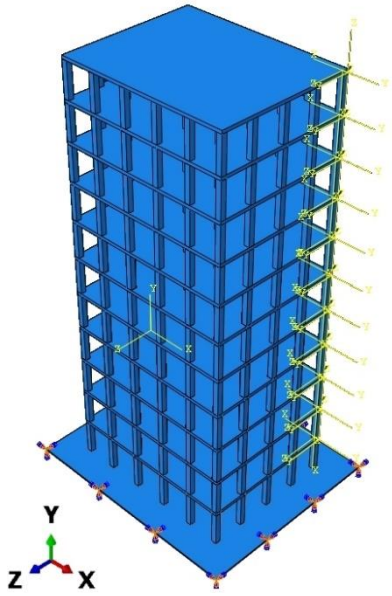

Figure 4.1.1: Example of a multi-story building frame model.

0.4.1 Model Description

3D FE models of the building frames using C3D8R elements were employed for the modal and dynamic analyses with very low displacement as inputs to simulate ambient vibrations and potential micro-tremors, Fig. 4.1.1. The building frames were categorized based on construction materials. The first group was constructed using Douglas-Fir wood, which is mainly used on lightweight buildings. The second group was constructed using GluLam wood, which for the purpose of this study was made of Douglas-Fir. The third frame group was constructed using GluLam columns and 7-layer CLT floors, which is a common method for tall mass-timber building construction. In this study CLT was made of Douglas-Fir. The previous materials were chosen to

compare and examine the modal characteristics of wood, its damping properties and the effect of fiber orientation on its dynamic behavior, while the fourth group was selected as a control group to compare with and evaluate the results from the wood analysis, and it was constructed using steel columns and concrete floors. The characteristics for every material are shown on Table 4.1.1.

Table 4.1.1: Mechanical material properties.

Material	Douglas-Fir	GluLam	Steel	Concrete
Humidity (*%*)	12	12	-	-
Damping (*%*)	3	3	3	5.5
Density (*Kg/m^3*)	530	530	7800	2400
E_1 (*GPa*)	13.86	15.29	200	30
E_2 (*GPa*)	0.69	0.76	-	-
E_3 (*GPa*)	0.94	1.04	-	-
ν_{12}	0.449	0.449	0.3	0.2
ν_{13}	0.292	0.292	-	-
ν_{23}	0.39	0.39	-	-
G_{12} (*GPa*)	1.08	1.19	-	-
G_{13} (*GPa*)	0.88	0.95	-	-
G_{23} (*GPa*)	0.09	0.1	-	-

Each frame material was tested at six different height configurations: 5, 7, 9, 11, 13 and 15 stories. The dimensions for the floors were 15m length, 12m width and 0.244m thickness; values that were selected based on the literature, Popovski and Gavric (2015), Hristovski et al. (2010). The thickness was determined from the construction of the 7-layer CLT slab, which is the maximum recommended thickness for CLT construction, United States Department of Agriculture (2013). Square columns were selected for simplicity. Their dimensions were 3m in height and 0.40m x 0.40m for the cross-section area. Traditional wood is not used in tall buildings; however, it was

necessary for the study's purpose, which was to compare traditional wood, composite wood with 0 degree fiber orientation and composite wood with 90 degree fiber orientation. Due to this limitation, to determine the wooden columns' cross section, we tested the frames' structural rigidity by gradually increasing the cross section until the 15-story frame was able to withstand 10% above its weight, and the dimension was kept the same for all the frames. This approach may produce unrealistic frame designs; however, we concluded that is the best way to investigate and compare the materials without having the geometry acting as another parameter for comparison.

The interactions at the joints where the columns and floors meet were defined having the nodes of each part constrained with the same displacements and rotations. This assumption is justified by the fact that the displacement due to loads used in the simulations are under the 0.8% of any dimension, therefore, the metal connectors can be simplified to simple constrains. For the implicit simulations, the buildings were placed on soil, represented by a fixed solid plate. The interaction between the columns and the soil was simulated as a movement restricted to no separation in Y-direction, and with tangential friction coefficient equal to 0.5, Canakci et al. (2016). The glue bonding in GluLam and CLT was modeled as interaction with movement restricted to no separation in Y-direction, and tangential friction coefficient equal to 1.0.

The loading for the modal dynamics analysis was applied on the main plane at the frames' fundamental frequency. The implicit dynamic analysis was performed having the building frames standing free on soil and the bottom nodes of the first floor's columns acted as input nodes where the impulse and the low amplitude earthquake loads were applied as boundary conditions.

4.2 Modal Analysis

The analysis of the four buildings begins with the natural frequency extraction using a modal analysis step. During this step, we get results for the first 25 vibration modes. After post-processing, the critical frequencies for each plane are identified based on their participation factor and the effective mass of the mode, Simulia (2014). Modal analysis is used to solve the free-vibration equation of motion expressed as,

$$M\ddot{u} + Ku = 0 \tag{4.2.1}$$

where M and K are the mass and stiffness matrices, and u denotes the generalized displacement,

$$u(t) = q_n(t)\varphi_n$$

where n is the number of modes, φ_n the deflected shape and $q_n(t)$ can be described by a simple harmonic function, resulting to the eigenvalue problem,

$$[K - \omega_n^2 M]\varphi_n = 0 \tag{4.2.2}$$

The solution will give the eigenvalue representing the natural frequencies ω^2 and the corresponding eigenvector φ_n as mode shape, Edskär (2018), Edskär and Lidelöw (2019).

4.3 Dynamic Analysis

4.3.1 Modal Dynamics

The dynamic analysis of the building is done in two steps. First, we investigate how the buildings respond to a vibration that is tuned on their natural frequencies; therefore, we apply a sinusoidal acceleration load of amplitude 0.001 m/s^2 tuned to the critical frequencies using a modal dynamics step. The total time of the simulation is selected to allow two complete mode periods. The governing equation of the modal dynamic analysis is described below.

$$\ddot{q}_\beta + C_{\beta\alpha}\dot{q_a} + \omega_\beta^2 q_\beta = f(t)_\beta \qquad (4.3.1.1)$$

For Equation 4.3.1.1, α, β are the eigenspace indices, $C_{\beta\alpha}$ the projected viscous damping matrix, q_β the generalized coordinate of the mode and $f(t)_\beta$ the magnitude of the load projected on this mode, Simulia (2014).

4.3.2 Implicit Dynamics

To investigate the buildings' response on ground vibrations we tested the building under two loads, an impulsive load and the El Centro earthquake. To ensure the linearity of the simulation, the magnitude of the signals was adjusted so the maximum displacement at any phase of the simulation is below 0.002 m. The duration of the simulations is 30 s, which was determined by the length of the El Centro acceleration data. Figure 4.3.2.1 shows a single-story building under excitation and

Equation 4.3.2.1, which is based on Newton's second law is the governing equation for the analysis.

$$[M]\ddot{x} + [C]\dot{x} + [K]x = F(t) \qquad (4.3.2.1)$$

where, *x* denotes the displacement vector and *M, C* and *K* are the mass, damping and stiffness matrices respectively.

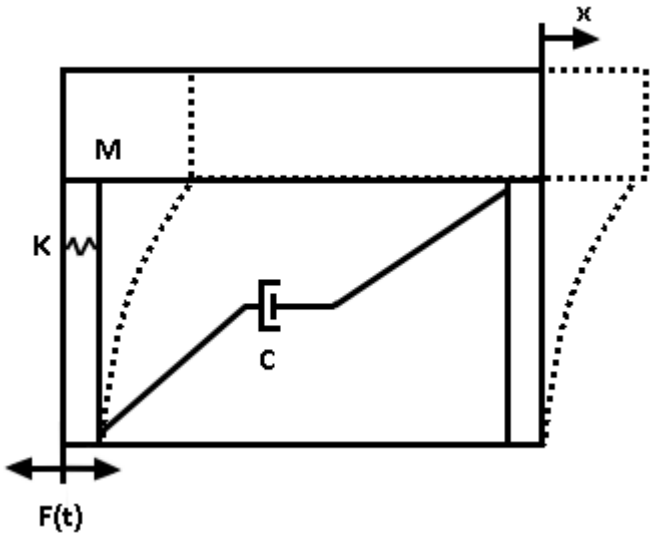

Figure 4.3.2.1: Example of a single-story building under excitation.

4.4 Theoretical Verification

The model validation for the isotropic materials concrete and steel was made using the analytical formula for a cantilever beam as shown in Equation 4.4.1.

$$f = \frac{k^2}{2\pi}\sqrt{\frac{EI}{ApL}} \tag{4.4.1}$$

where, *f* is the resonance frequency, *k* is a dimensionless correction parameter for each mode, which is equal to 1.875 for the first mode. *E* is the material stiffness, *I* is the second moment of inertia, *A* is the cross-section area, *p* is the density and *L* is the length of the cantilever.

The orthotropic materials Douglas-Fir and GluLam were validated using the measurements in Guan et al. (2017). The study provides experimental laboratory measurements for the first nine natural modes of wood composite panels. The information in the study allowed for the creation of FEA models to simulate the experiments. Finally, the CLT modeling was verified using the measurements in Weckendorf et al. (2016). The material properties provided by the authors described the CLT as a homogeneous slab, not as individual wood slabs, thus, for the verification we used material properties from the literature based on the wood family the authors provided in the study. Table 4.4.1 shows the comparison between the theoretical (experimental) and the FEA results. Steel and concrete compare very well with the theoretical values. The results from the wood product validation, showed variations less than 5%, with only one measurement reaching 11.1%. It is important to note that for the orthotropic and the CLT models, there was a deviation from the actual material

properties and boundary conditions the authors used. For instance, the boundary conditions were estimated from the figures in the publications. Due to these modeling differences, we estimate that the deviation from the study's values is higher than expected. Nevertheless, based on the overall low error percentages, we concluded that the framework and the models can provide useful results.

Table 4.4.1: Theoretical and numerical calculated natural frequencies.

$Material_{mode}$	**Theoretical (Experimental)**	**FEA (Hz)**	**Difference (%)**
$Steel_1$	22.1	21.6	2.2
$Concrete_1$	15.4	15.1	1.9
MDF_1	4.7	4.7	0.0
MDF_2	8.67	9.01	3.9
MDF_3	12.5	12.4	1.0
MDF_4	14.2	14.7	3.3
MDF_5	15.6	16.1	3.5
MDF_6	16.9	18.0	6.7
MDF_7	19.1	19.2	0.4
MDF_8	22.3	22.2	0.4
MDF_9	30.7	30.6	0.4
CLT_1	12	12.03	0.2
CLT_2	19.7	21	6.6
CLT_3	41.7	43.43	4.1
CLT_4	51.4	53.45	4.0
CLT_5	77.7	86.36	11.1
CLT_6	91.8	84.91	7.5

Chapter 5: Results and Analysis

5.1 Frequency Extraction

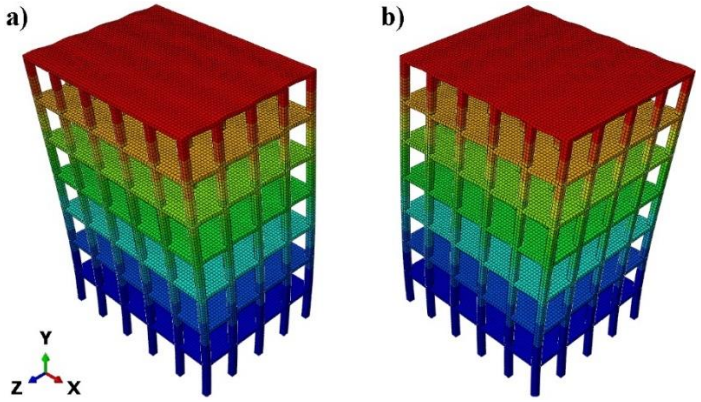

Figure 5.1.1: The first (a) and second (b) mode shape for each building frame.

The analysis framework begins extracting the natural frequencies of each frame using modal analysis. Figure 5.1.1 shows the first and second natural mode-shapes for the frames, and Figure 5.1.2 presents the first two resonance frequencies for each frame based on its material and height. The results show that the frames made from Douglas-Fir and GluLam have natural frequencies frequencies between 0.38 - 0.48Hz and the steel-concrete frame resonate at frequencies around 0.7 - 0.8Hz. GluLam-CLT frames resonated at higher frequencies than the other materials at a range between 1.25 - 1.35Hz. Furthermore, Figure 5.1.2 reveals a common trend about the resonance frequency for each mode, which decreases as the height increases. However, the slope of the decrement is not the same for all the materials. The GluLam-CLT frames start with a small slope for the 5 and 7-story frames, but for higher frames the frequencies for both modes decrease rapidly as the height increases. On the other hand, the steel-

concrete frame has a steeper decrement slope beginning at the 5-story frame until the 9-story frame, and then it follows a smoother decrement for higher frames. The trend for the first mode for the Douglas-Fir and GluLam frames compares closely to the GluLam-CLT but at lower frequencies. However, for the second mode, the frequencies follow a trend similar to the steel-concrete frame.

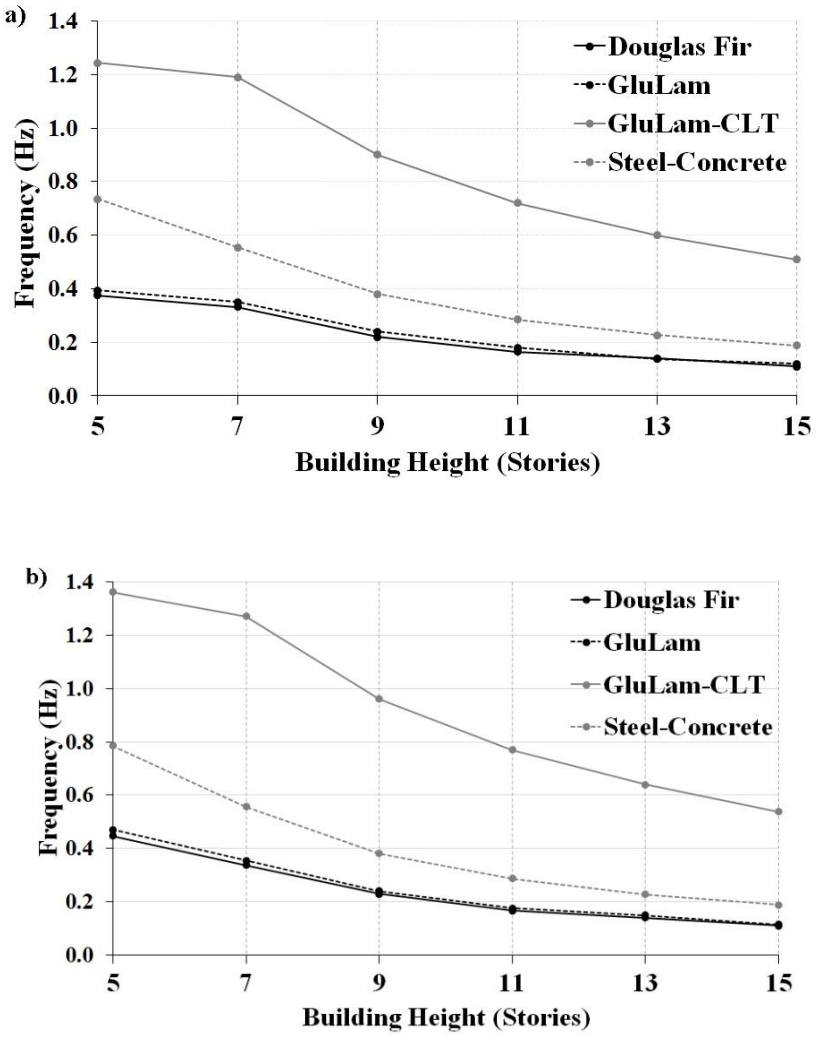

Figure 5.1.2: The first (a) and second (b) mode for each building frame.

5.2 Resonance Response

To calculate the frames' maximum displacement when in resonance, the load for the modal dynamics analysis is tuned at each frame's strongest mode, which was found on the previous step. To ensure that the forces acting on the frames were in the linear stress/strain zone, we restrict the oscillation only to 2 periods duration, resulting to displacements less than 10% of the frames' minimum dimension. Figure 5.2.1 summarizes the frame's displacements, revealing that frames constructed from Douglas-Fir and GluLam wood exhibit larger displacements than the other frames with values 0.019m and 0.017m respectively for the 15-story frame. The steel-concrete frame reached 0.006m displacement for the 15-story frame and lastly the GluLam-CLT 15-story frame demonstrated the lowest displacement at 0.001m.

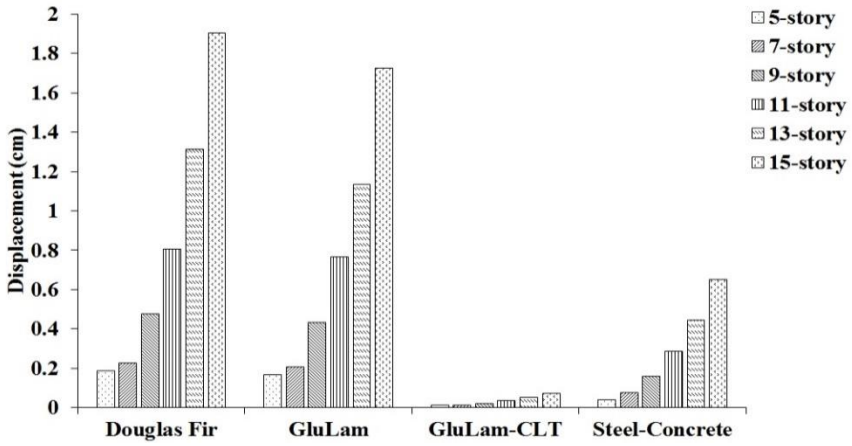

Figure 5.2.1: Amplitude of each frame after 2 periods of vibration.

5.3 Impulse Response

Next, we performed an implicit dynamics analysis using an impulse signal as input. After post-processing the results using the logarithmic decrement method, we calculated the hysteresis damping ratio for each frame. Douglas-Fir and GluLam frames showed similar ratios around 2%, steel-concrete frames showed ratios which reach 4% and the GluLam-CLT frames showed the highest damping ratios reaching 5%, Fig. 5.3.1. Figures 5.3.2 and 5.3.3 show the detailed impulse responses for all the frames. A common trend between the Douglas-Fir, the GluLam and the steel-concrete frames is that the vibration's amplitude and complexity due to multiple mode shapes increase with the increase of the height. The GluLam-CLT frame, however, exhibited similar, simpler oscillation through-out all the heights.

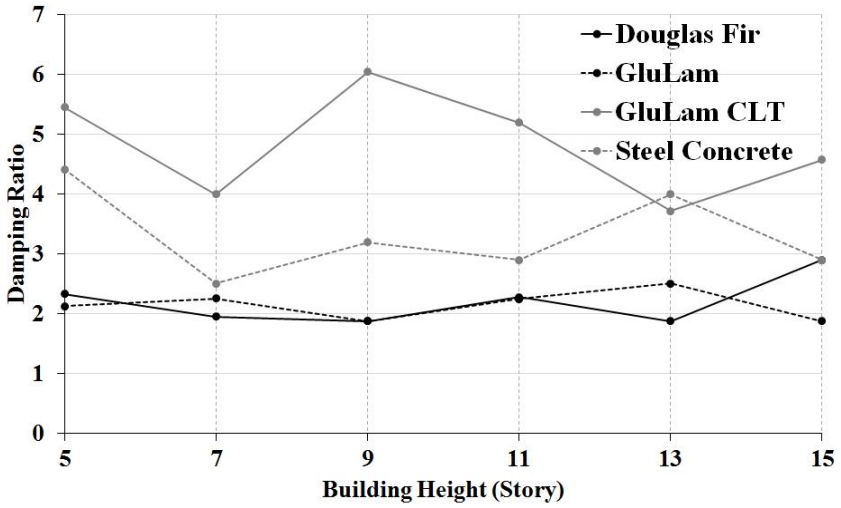

Figure 5.3.1: Damping ratios for each frame.

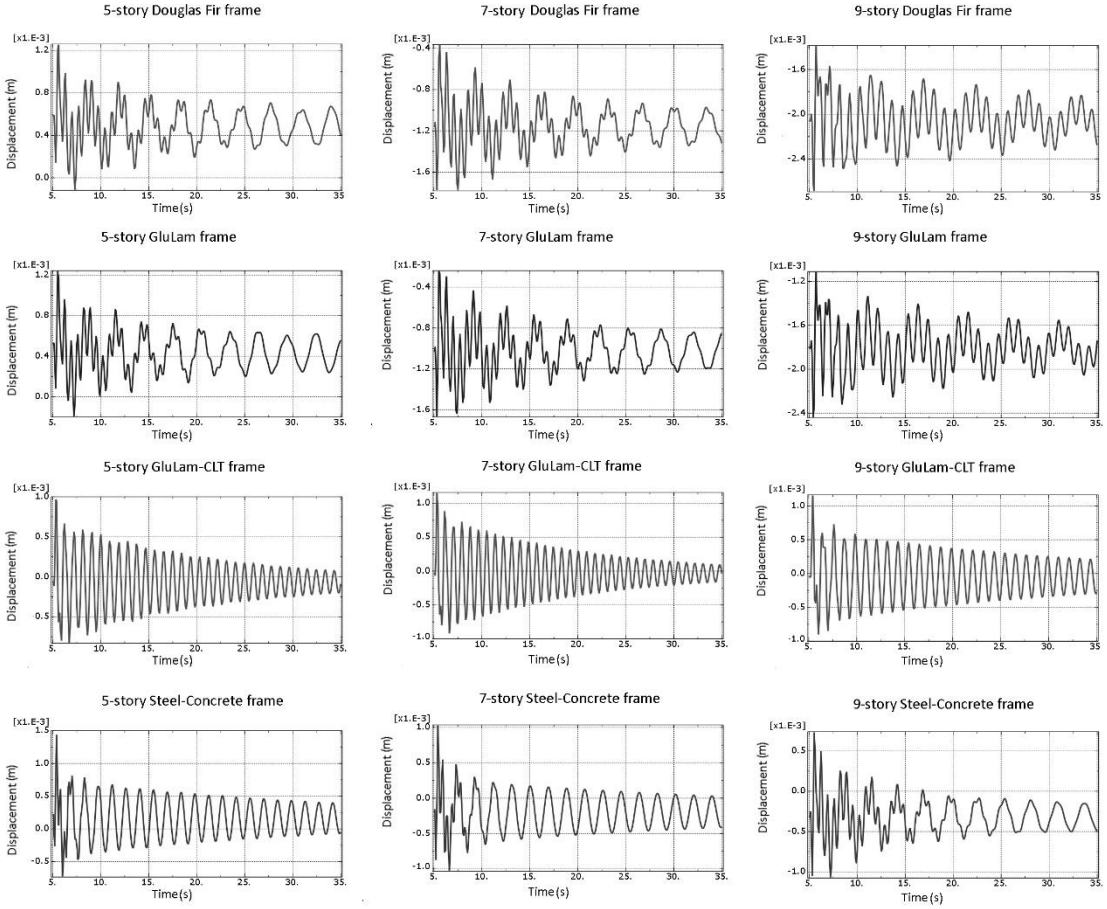

Figure 5.3.2: Impulse response of the 5, 7 and 9-story building frames.

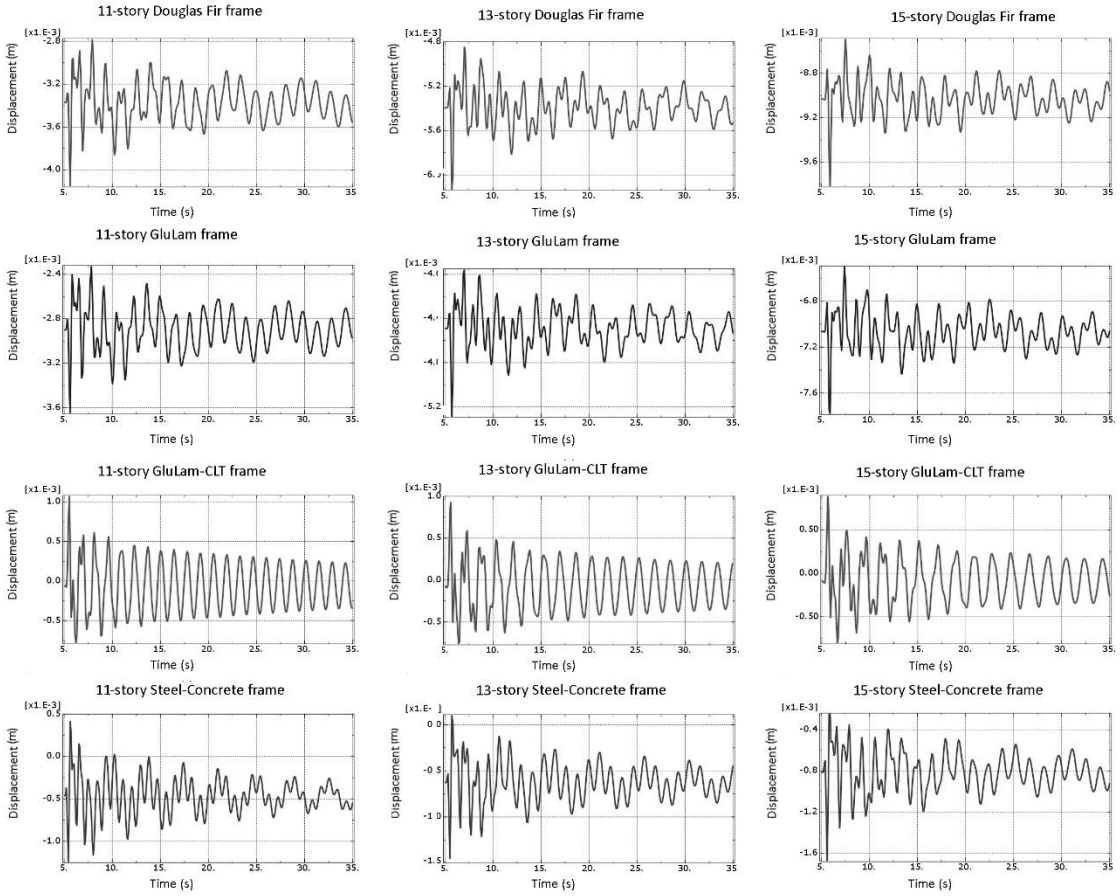

Figure 5.3.3: Impulse response of the 11, 13 and 15-story building frames.

To further quantify the frames' impulse response, we examine the displacement attenuation at the end of the experiment (i.e. in 30 seconds timeframe). The results presented in Figure 5.3.4 reveal that frames with higher stiffness made of GluLam-CLT and steel-concrete exhibited greater attenuation over time than frames made of low stiffness materials. No trends were found for the frames made of Douglas-Fir and GluLam. However, the results from the frames made of high stiffness materials, indicate that a trend may exist. In detail, the GluLam-CLT frames showed low attenuation for the 5-story frame, which then increased for the 7-story frame and gradually decreased as the frame's height increased. The steel-concrete frame showed high attenuation for the 5-story frame which slowly decreased as the height increased, reaching the lowest values around 0.0007m for the 11, 13 and 15-story frames.

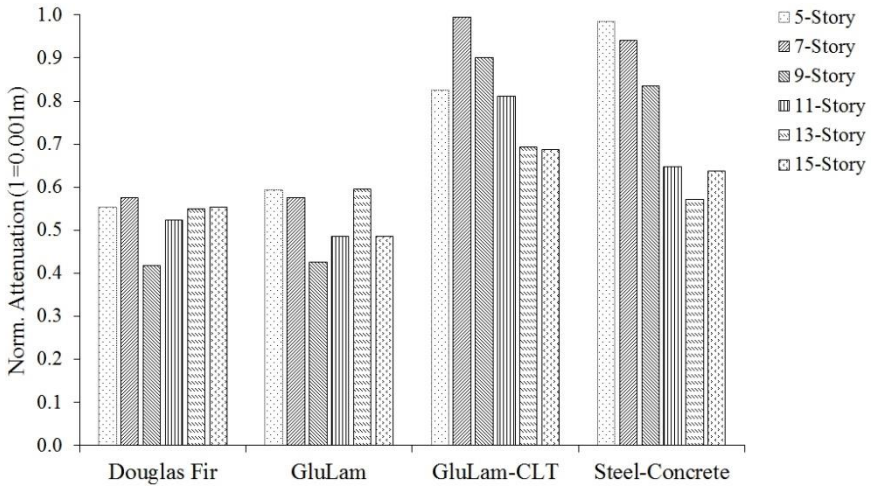

Figure 5.3.4: Displacement attenuation for each frame in 30s timeframe.

Lastly, we present a Roof-displacement/Ground-input ratio, which shows the relationship between the maximum displacement measured at the roof story of each frame and the input displacement at the first story columns. The results in Figure 5.3.5 reveal that the $Roof_{displacement}/Ground_{input}$ ratio chart looks similar to the displacement attenuation chart from the previous step, but with less variation between frames at different height. Douglas-Fir and GluLam frames demonstrated input-output ratio averaging at 0.55. GluLam-CLT and steel-concrete frames resulted to an average ratio of 0.8.

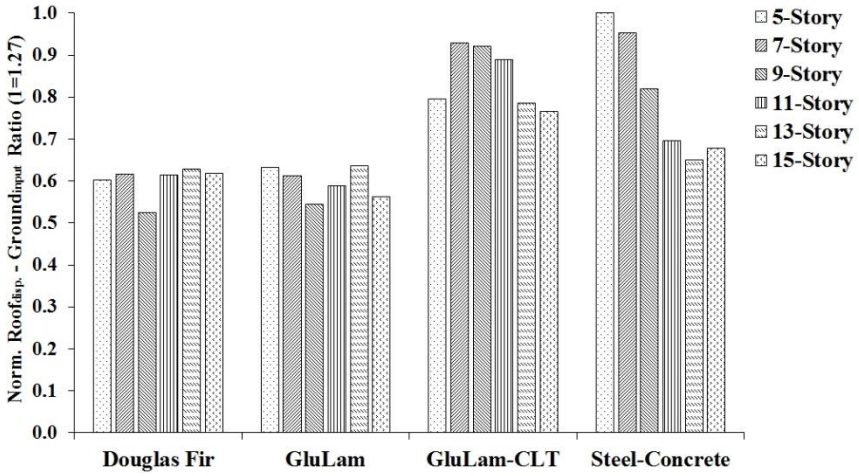

Figure 5.3.5: $Roof_{displacement}/Ground_{input}$ ratio for each frame.

5.4 Earthquake Response

The final test was performed to observe how the frames respond to a random excitation, such as micro-tremors or winds. We applied the scaled El-Centro earthquake signal as an input to the frames, Fig. 5.4.4. The earthquake's data can be found online, El Centro Earthquake Page. Figure 5.4.2 and Figure 5.4.3 show the detailed behavior

for all the frames. Figure 5.4.1 shows the largest displacement each frame reached during the earthquake according to its height. The results suggest that there is no linear correlation between the frames' height and the displacement. However, a common characteristic between Douglas-Fir, GluLam and steel-concrete frames is that there is one frame from each material group that exhibited very high displacement. We estimate that the earthquake signal may include a frequency close to a resonant frequency of those frames. On the other hand, the GluLam-CLT frames did not show similar behavior, and they also exhibited lower peak displacement than the other frames. The averaged displacements for each material was Douglas-Fir: 5.5cm, GluLam: 5.9cm, GluLam-CLT: 3.4cm and steel-concrete: 5.3cm

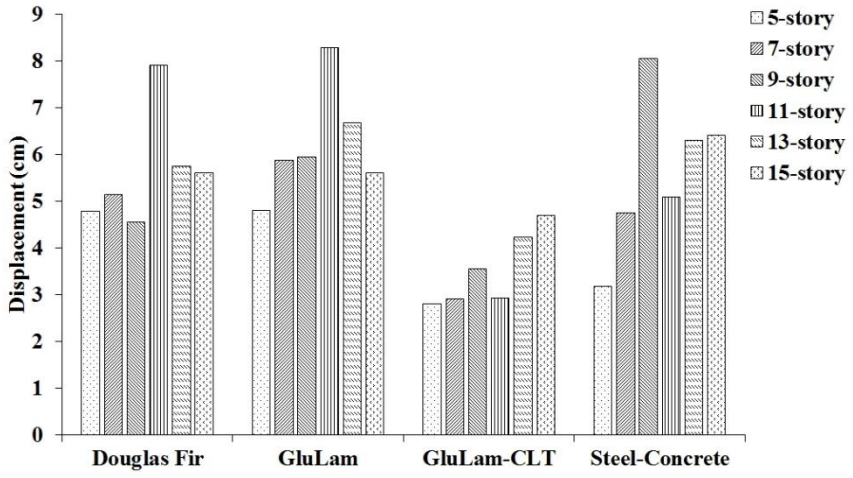

Figure 5.4.1: Maximum displacement for each frame under the El Centro excitation.

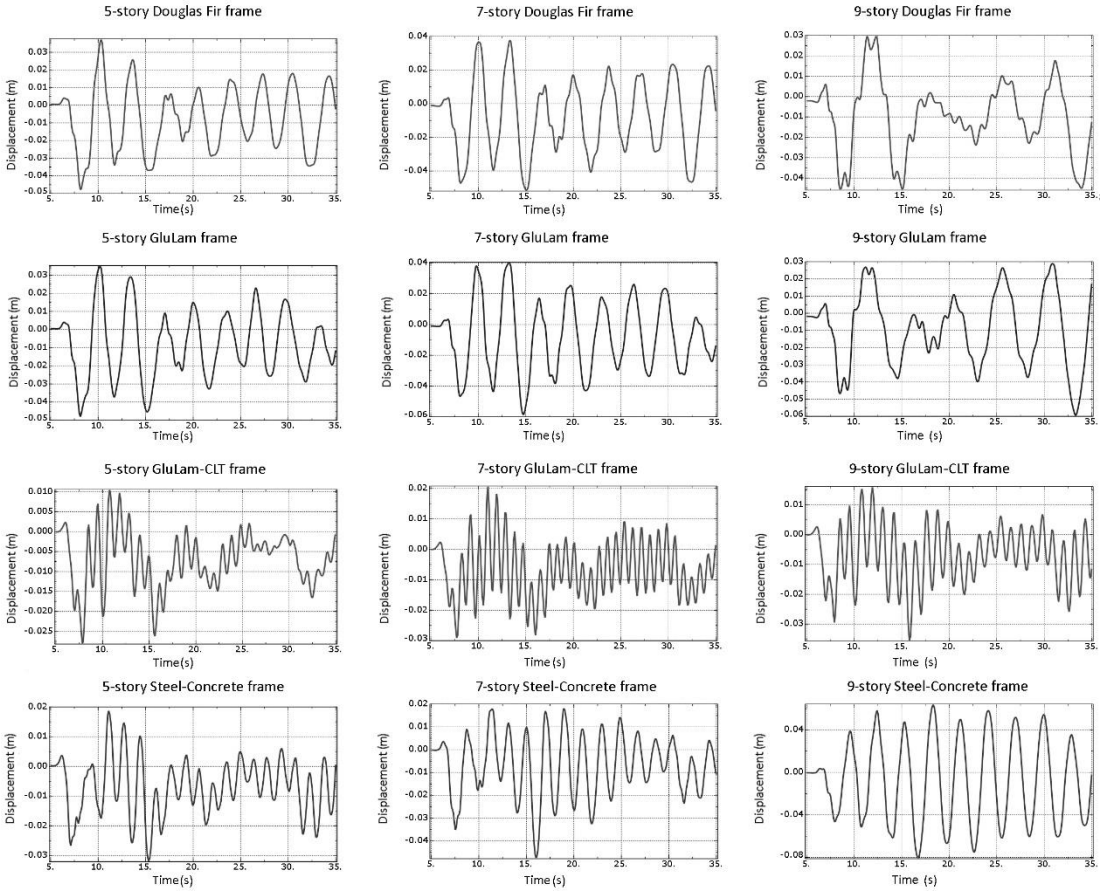

Figure 5.4.2: Earthquake response of the 5, 7 and 9-story building frames.

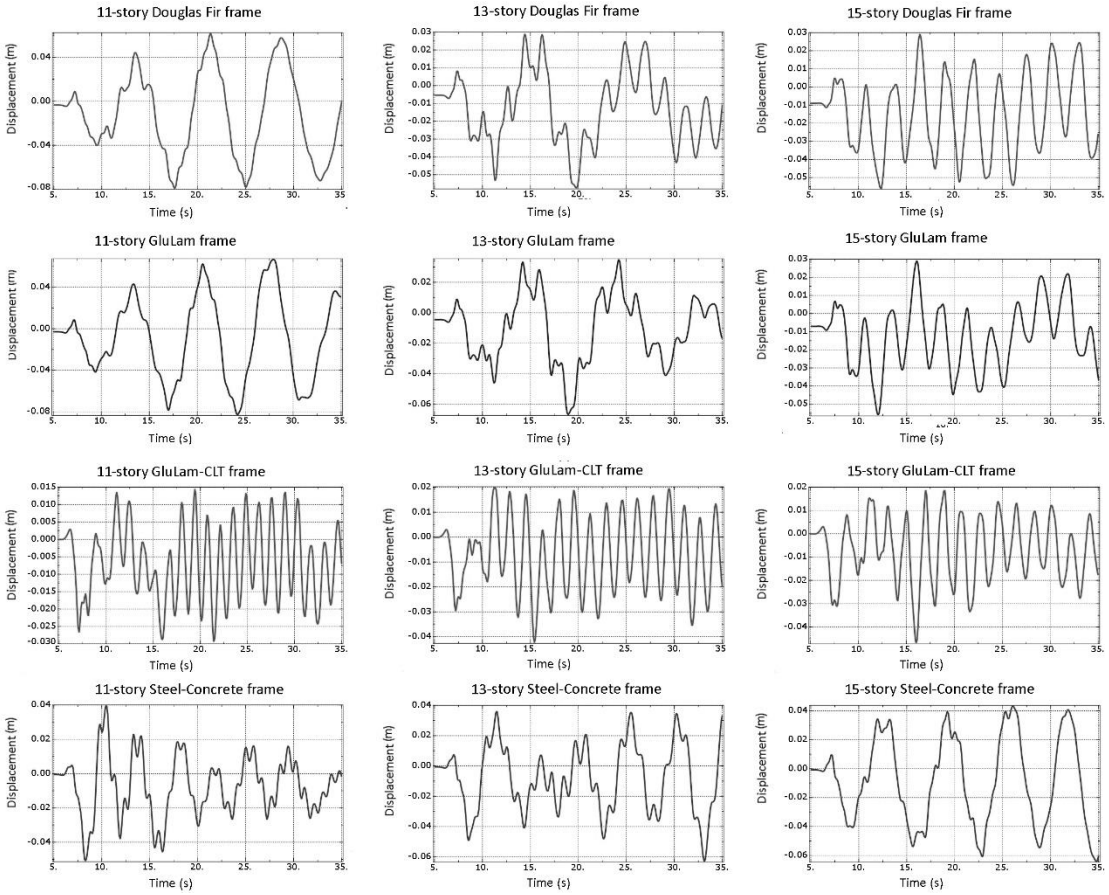

Figure 5.4.3: Earthquake response of the 11, 13 and 15-story building frames.

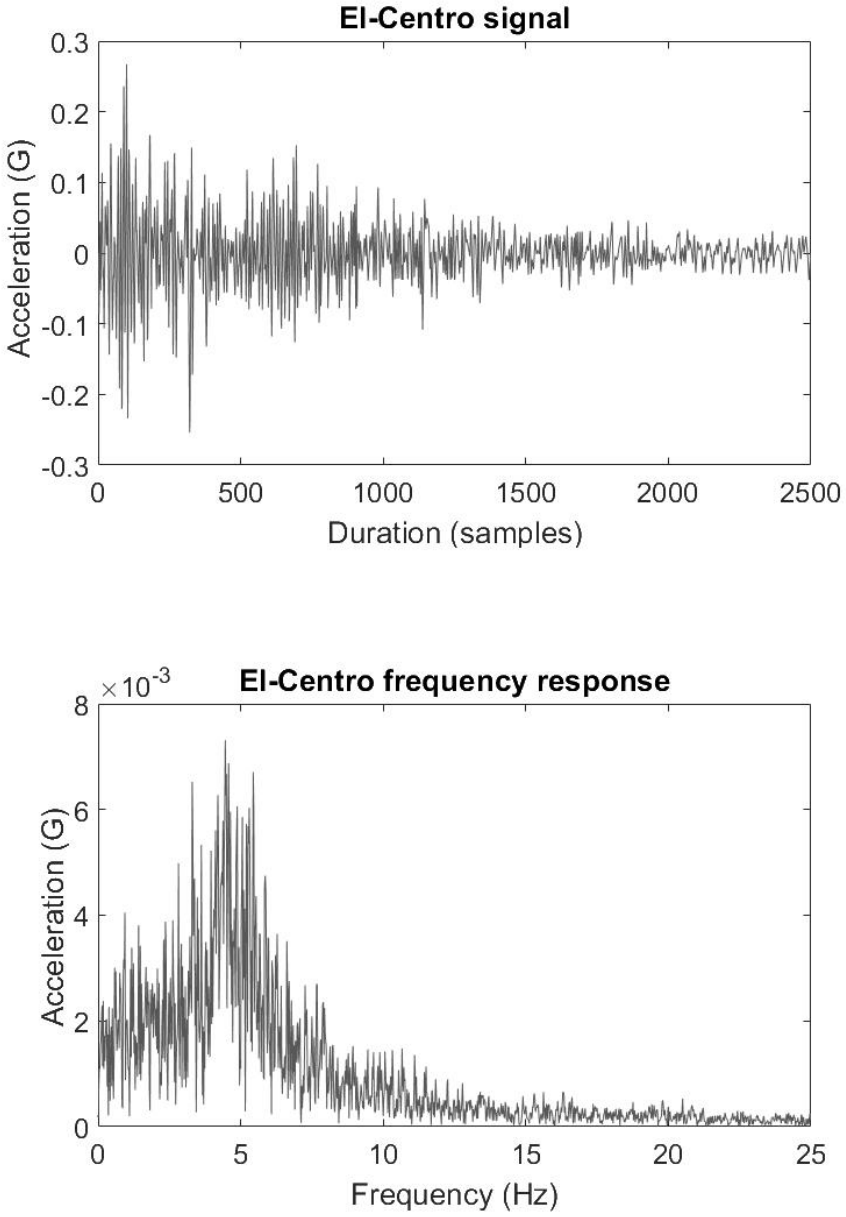

Figure 5.4.4: The El Centro earthquake data.

Chapter 6: Discussion and Conclusion

The study reveals important information related to mass-timber wood products and the fiber orientation effects on natural frequencies, damping and dynamic response. The results from the experiments show that fiber orientation has greater effect on the structures' natural modes than the effect from increasing strength, resulting to resonances at frequencies 3x times higher than the frequencies when the fiber orientation is the same between the wood layers and 1.7x times higher than the steel-concrete frame. Furthermore, for the GluLam-CLT frames, the slope of the frequency decrement due to height differs between low and high frames, a phenomenon that may reveal increased stiffness at low height frames. The displacement measurements when the frames are in resonance show that GluLam-CLT frames outperform other frames at every height, resulting to displacements multiple times lower. This behavior suggests that when the fiber-discontinuity is introduced from exchanging the fiber orientation, may increases the time for the frame to reach maximum displacement. The displacement attenuation and the $Roof_{displacement}/Ground_{input}$ ratio results reveal that stiffer material combinations, such as GluLam-CLT and steel-concrete result in higher numbers than low-stiffness materials, which translates they allow to vibration signals to propagate with less attenuation through the frame. However, the frames tend to mitigate these vibrations fast preventing accumulation of displacement. This suggests that an inverse correlation between the damping ratio and the vibration propagation may exist; however, more research is needed to form solid conclusions. Changing material properties similar to the example of Douglas-Fir and GluLam does not affect the damping ratio, but when the fiber orientation changes, the damping ratio increases. Another interesting outcome is that the height of the frames does not affect the hysteresis damping ratio, the impulse response nor the response to random signals. Lastly, the

experiments revealed that the fiber orientation has great impact on the dynamic behavior of the frames resulting to controlled movement which follows closely the shape of the input signal.

Chapter 7: Conclusion and Future Work

Summing the multi-analysis examination of the mass-timber wood products, this study complements the previous work showing behavior trends rising from the systematic multi-specimen simulation. The study suggests that GluLam and CLT when combined may exhibit comparable results or even outperform traditional materials, including steel and concrete. However, the high frequency vibrations that the GluLam-CLT frames show, suggest that additional research is required to examine the materials in detail and ensure compliance with the standards for resident comfort. The difference between the results from the GluLam (0^o) and the GluLam-CLT (90^o) frames suggests that there is ground for fine-tuning the fiber orientation angle and meet the modern buildings' construction requirements.

Future work may include an optimization studies which will examine the effect that thickness of the individual wood planks has on the dynamic properties of the structures. Moreover, the fiber orientation angles may be calculated based on their vibration range damping properties for structural stability and resident comfort.

Bibliography

Amini Y., Heshmati M., Fatehi P. and Habibi S.E. (2017) “Piezoelectric energy harvesting from vibrations of a beam subjected to multi-moving loads”. Applied Mathematical Modelling, 49, pp. 1-16.

Asdrubali F., Ferracuti B., Lombardi L., Guattari C., Evangelisti L. and Grazieschi G. (2017) “A review of structural, thermo-physical, acoustical, and environmental properties of wooden materials for building applications”. Building and Environment 114, pp. 307-332, doi: 10.1016/j.buildenv.2016.12.033.

Bathe K.-J. (2014) “Finite Element Procedures, Second Edition”. Book.

Canakci H., Hamed M., Celik F., Sidik W. and Eviz F. (2016) “Friction characteristics of organic soil with construction materials”. Soils and Foundations, 56 (6), pp. 965-972, doi: 10.1016/j.sandf.2016.11.002.

Edskär I. (2018) “Modal Analysis, Dynamic Properties, and Horizontal Stabilisation of Timber Buildings”. Luleå University of Technology, Department of Civil, Environmental and Natural Resources Engineering.

Edskär I. and Lidelöw H. (2019) “Dynamic properties of cross-laminated timber and timber truss building systems”. Engineering Structures, 186 pp. 525–535, doi: 10.1016/j.engstruct.2019.01.136

El Centro Earthquake Page, http://www.vibrationdata.com/elcentro.htm. Online

Frei W. (2013), https://www.comsol.com/blogs/how-identify-resolve-singularities-model-
meshing/. Online

Garikipati K. (2014) “Intoduction to Finite Element Methods”. https://www.youtube .com/watch?v=U65GK1vVw4o&list=PLJhG_d-Sp_JHKVRhfTgDqbic_4MHpltXZ& index=2. Online

Gsell D., Feltrin G., Schubert S., Steiger R. and Motavalli M. (2007) “Cross-laminated timber plates: Evaluation and verification of homogenized elastic properties”. Journal

of Structure Engineering, 133 (1), pp. 132-138, doi:10.1061/(ASCE)0733-9445(2007)133:1(132).

Guan C., Zhang H., Wang X., Miao H., Zhou L. and Liu F. (2017) "Experimental and theoretical modal analysis of full-sized wood composite panels supported on four nodes". Materials, 10 (683), doi:10.3390/ma10060683.

Hristovski V., Dijic B., Stojmanovska M. and Mircevska V. (2010) "Full-scale shaking-table tests of xlam panel systems and numerical verification: Specimen 1". Journal of Structure Engineering, 139 (11), doi:10.1061/(ASCE)ST.1943-541X.0000754.

Hu L, Omeranovic A, Gagnon S and Mohammad M. (2014) "Wind-induced vibration of tall wood buildings–is it an issue?". Wolrd conference on timber engineering, Quebec City, Canada.

Hyun K.D. and Young K.J. (2014) "Assessment on natural frequencies of structures using field measurement and FE analysis". International Journal of High-Rise Buildings, 3 (4), pp. 305-310.

Izzi M., Casagrandea D., Bezzib S., Pascac D., Follesad M. and Tomasi R. (2018) "Seismic behaviour of Cross-Laminated Timber structures: A state-of-the-art review". Engineering Structures, 170 pp. 42–52, doi: 10.1016/j.engstruct.2018.05.060

Jarnero K., Brandt A. and Olsson A. (2010) "Vibration properties of a timber floor assessed in laboratory and during building construction". Internoise.

Kawecki J. and Kowalska A. (2011) "Analysis of vibration influence on people in buildings in standards approach". Transactions on Ecology and The Environment, 148, doi: 10.2495/RAV110331

Kawecki J., Kowalska A. and Stypula K. (2011) "Consideration of Criteria of Vibration Comfort of People in Diagnosis and Design of Buildings". Engineering and Technology, 59.

Maldonado S.A.H. and Chui Y.H. (2014) "Effect of end support conditions on the vibrational performance of cross-laminated timber floors". World conference of Timber Engineering.

MatWeb, http://www.matweb.com/search/DataSheet.aspx?MatGUID=d6401be500

16459dada858cb6e0f7eb6, Online

Mugabo I., Barbosa A.R., Riggio M. and Batti1 J. (2019) “Ambient Vibration Measurement Data of a Four-Story Mass Timber Building”. Frontiers in Built Environment, doi:10.3389/fbuil.2019.00067.

Popovski M. and Gavric I. (2015) “Performance of a 2-story clt house subjected to lateral loads”. Journal of Structure Engineering, 142, doi:10.1061/(ASCE)ST.1943-541X.0001315.

Quang Mai K., Park A., Nguyen K.T., Lee K. (2018) “Full-scale static and dynamic experiments of hybrid CLT-concrete composite floor”. Construction and Building Materials, 170 pp. 55–65, doi: 10.1016/j.conbuildmat.2018.03.042

Reynolds T, Bolmsvik Å, Vessby J, Chang W-S, Harris R and Bawcombe J, (2014) “Ambient vibration testing and modal analysis of multi-storey cross-laminated timber buildings”. World conference on timber engineering, Quebec City.

Raynolds T., Harris R., Chang W.S., Bregulla J. and Bawcombe J. (2015) “Ambient vibration tests of a cross-laminated timber building”. Construction materials, 168, pp. 121-131.

Sandhaas C. and Ceccotti A. (2012) “Earthquake resistance of multi-story massive timber buildings”. Forum Holzbau Beaune, 12.

Sato M., Isoda H., Arakic Y., Nakagawad T., Kawaie N. and Miyake T. (2019) “A seismic behavior and numerical model of narrow paneled cross-laminated timber building”. Engineering Structures, 179, pp. 9-22, doi: 10.1016/j.engstruct.2018.09.054.

Schiavia A. and Rossi L. (2015) “Vibration perception in buildings a survey: From the historical origins to the present”. Energy Procedia, 78, pp. 2-7, doi: 10.1016/j.egypro.2015.11.094.

Simulia (2014) “Abaqus Theory Guide”. pp. 2.5.2.

The engineering toolbox, https://www.engineeringtoolbox.com/concrete-properties-d_1223.html, Online.

United States Department of Agriculture (2010) “Wood handbook, Wood as an engineering material”.

United States Department of Agriculture (2013) “CLT handbook, Cross laminated timber”.

Ussher E., Arjomandi K., Weckendorf J. and Smith I. (2017) “Predicting effects of design variables on modal responses of CLT floors”. Structures, 11, pp. 40-48.

Ussher E., Arjomandi K., Weckendorf J. and Smith I. (2017) “Prediction of motion responses of cross-laminated-timber slabs”. Structures, 11, pp. 49-61.

Ventura C.E., Lord J.F., Turek M., Brincker R., Andersen P. and Dascotte E. (2005) “FEM updating of tall buildings using ambient vibration data”. Structure Dynamics EURODYN, 19 (4-7), pp. 237-242.

Weckendorf J. Ussher E. and Smith I. (2016) “Dynamic response of CLT plate systems in the context of timber and hybrid construction”. Composite Structures, 157 (1-12), pp. 412-423.

Wei C. and Jing X. (2017) “A comprehensive review on vibration energy harvesting: Modelling and realization”. Renewable and Sustainable Energy Reviews, 74, pp. 1-18, doi: 10.1016/j.rser.2017.01.073